ChemComm

Accepted Manuscript

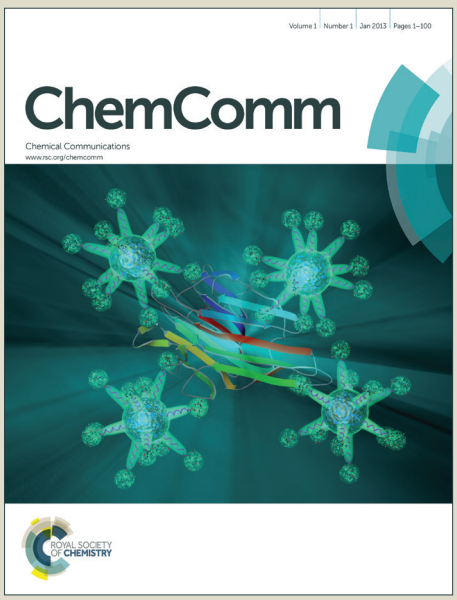

ROYAL SOCIETY OF CHEMISTRY

www.rsc.org/chemcomm

Chemical Communications ChemComm

Dynamic Article Links ►

Cite this: DOI: 10.1039/c0xx00000x

www.rsc.org/xxxxxx

ARTICLE TYPE

Synthesis of highly monodisperse porous manganese oxide spheres using a butyric acid microemulsion

Stanton Ching,*[a] Ian J. Richter,[a] Kathryn A. Tutunjian,[a] David A. Kriz,[a,b] and Yumi Kovic[a]

Received (in XXX, XXX) Xth XXXXXXXXX 20XX, Accepted Xth XXXXXXXXX 20XX

DOI: 10.1039/b000000x

Porous manganese oxide spheres form readily from a reaction between $KMnO_4$ and n-butanol in aqueous butyric acid under ambient conditions. Spheres have uniform size, tuneable diameters and high surface areas. The material is an active catalyst for the oxidation of isopropanol to acetone.

Porous manganese oxides continue to attract considerable interest as promising materials for heterogeneous catalysis, battery and electrochemical applications, and toxic waste remediation.[1-3] Many crystalline and amorphous forms are known, including those with spherical and hollow spherical structures comprised of aggregated nanoparticles.[4-17] Such hierarchical morphologies often result in high surface areas that are desirable in applications where interfacial contact is critical.

We previously described the use of butyric acid (BA) as an easily removed soft template to prepare manganese oxide hollow spheres with high surface areas.[4] In aqueous reactions between $KMnO_4$ and $MnSO_4$, BA serves as a capping ligand that supresses manganese oxide particle growth on the nanoscale, while simultaneously forming a microemulsion that enables the resulting nanoparticles to aggregate into hollow spheres. Herein we report further research on BA as a template for hierarchical manganese oxide. Its presence in reactions between $KMnO_4$ and n-butanol (BuOH) results in highly uniform and porous (but not hollow) spheres. This facile, one-pot reaction occurs under ambient conditions.

Porous manganese oxide spheres form as a brown precipitate within 20 minutes of adding 25 mL of aqueous 0.040 M $KMnO_4$ to a 25 mL aqueous mixture of 0.48 M BuOH and 1.0 M BA. The reaction is carried out at room temperature under atmospheric pressure, S1. About 80 mg is typically obtained after filtration, washing, and drying at 110 °C. The material is amorphous based on powder XRD, S2. A formula of $K_{0.027}MnO_{1.88}\cdot 0.61H_2O$ was determined by AA (for K and Mn) and TGA (for waters of hydration). From this formula, the isolated yield is about 80% based on Mn. Thiosulfate/iodide redox titration was used to determine an average Mn oxidation state of 3.59. FT-IR shows no evidence of residual BA.

SEM and TEM images reveal highly monodisperse spheres, with average diameters measuring 379±15 nm, Fig. 1. TEM reveals spheres consisting of nanoplatelets, as seen on surfaces in Figure 1B. The distribution of sphere diameters is shown in Fig. 2. The hierarchical structure and morphology are consistent with the high surface area of 243 m^2/g measured by BET analysis. Nitrogen adsorption/desorption shows type-IV isotherm behavior, characteristic of a mesoporous material, S3. Pore size distribution calculated by the BJH method revealed three distinct meso-range distributions, with a major peak at 4.88 nm, followed by peaks at 3.83 nm and 2.18 nm, S4. HRTEM images reveal mesoporosity, as well as short range order that is typical for amorphous maganese oxides, Fig. 3. Platelet size is about 10 nm. Control reactions without BA result in loss of the spherical morphology and formation of larger aggregated particles, Fig. 4. Surface area for the control is 139 m^2/g.

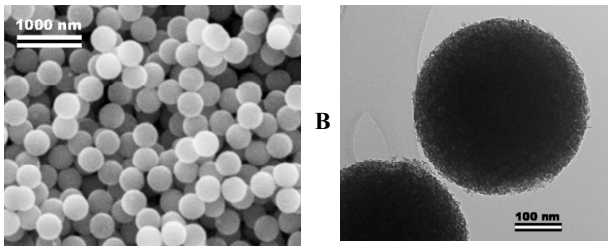

Fig. 1. (A) SEM and (B) TEM images of porous manganese oxide spheres from $KMnO_4$ and BuOH in the presence of BA (S1).

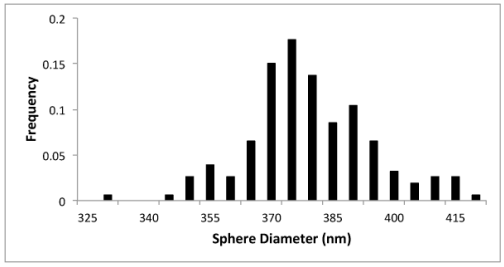

Fig. 2. Size distribution for porous manganese oxide spheres (S1) with average diameter of 379 nm.

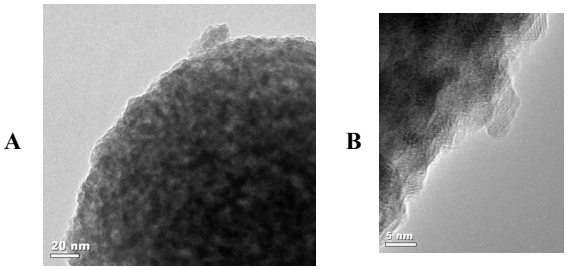

Fig. 3. HRTEM images of a porous manganese oxide sphere (S1) showing (A) mesoporosity and (B) short range order in the nanoplatlets.

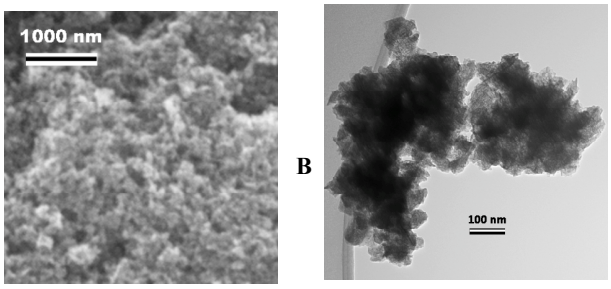

Fig. 4. (A) SEM and (B) TEM images manganese oxide from the control reaction of $KMnO_4$ and BuOH without BA. (S1 without BA)

Sphere size is responsive to $KMnO_4$ concentation, which allows the tuning of sphere diameters between 267 and 633 nm, Fig. 5. High surface areas of 176-256 m^2/g are maintained for the different sphere sizes, S5. Larger diameters can be obtained with higher $KMnO_4$ concentrations, but there is considerable loss of monodispersity, S6.

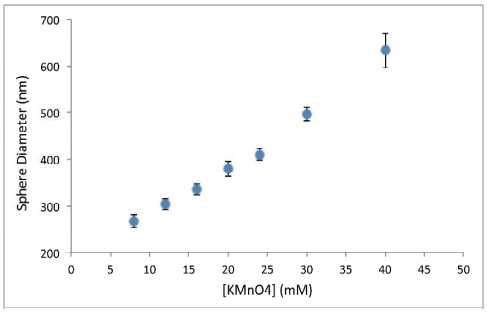

Fig. 5. Plot of sphere diameter vs. [$KMnO_4$] used in each reaction.

Porous manganese oxide spheres are stable to prolonged stirring, sonication, and reflux. However, the spheres are crushed under high compression (10 tons). Thermal stability measured by TGA shows gradual weight loss of 12% from 40 °C to 230 °C due to loss of adsorbed water, Fig. 6A. From 230 °C to 475 °C, a more gradual change of 4% is attributed to the loss of more strongly adsorbed water and chemisorbed O_2.[18] The sharp transition at 475 °C corresponds to loss of O_2 and concomitant formation of Mn_2O_3, as confirmed by XRD. Surface area measured after calcination at 500 °C shows dramatic decrease to 32 m^2/g. Sintering is observed as the amorphous nanoplatelets convert to crystalline Mn_2O_3, even while the overall spherical motif is retained, Fig. 6B.

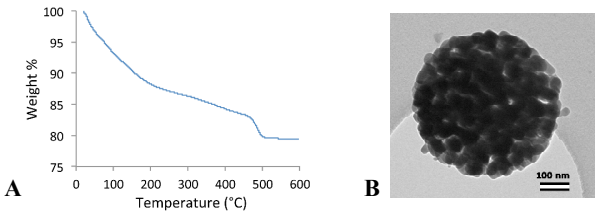

Fig. 6. (A) TGA analysis of porous manganese oxide spheres. (B) TEM image after calcination at 500 °C. Samples prepared as in S1.

There are numerous routes to spherical manganese oxides, though the quality of spherical structures and ease of preparation varies considerably. Self assembly syntheses are facile, but do not yield the precise control over size and shape reported here.[5-8] The same holds for hydrothermal treatment, which additionally requires more forcing conditions to promote Ostwald ripening.[8-11] Use of hard templates such as silica, carbon, polymer and $MnCO_3$ spheres yield highly uniform hollow spheres, but require lengthier procedures to introduce, then dissolve, the template.[12-15] The system we report here offers a combination of features that make it distinct from other synthetic manganese oxides: (1) spheres are well formed and highly monodisperse; (2) sphere size can be controled with good precision; (3) reaction occurs readily under ambient conditions; (4) porosity resulting from aggregated nanoplatelets delivers very high surface area.

This research grows out of our broader efforts to develop synthetic routes to nanoparticle manganese oxides having high surface areas. Our work is inspired by the chemistry of $[Mn_{12}O_{12}(O_2CCH_3)_{16}(H_2O)_4]$ clusters and related molecular systems.[13] The clusters have cores of MnO_6 octahedral units, similar to those of manganese oxide materials, but are stabilized by coordinated acetate ligands.[19] In our nanoparticle system, we propose that BA coordinates weakly enough so that molecule-size clusters are uninhibited from growing into larger material-size particles. Weak coordination also allows easy removal of BA by washing. However, BA coordinates strongly enough to cap manganese oxide growth on the nanoparticle scale. The nanoparticles then aggregate to form a hierarchical structure. Coordinating solvents have been reported to function as ligands in syntheses of Mn_3O_4, also resulting in reduced particle size.[20]

A proposed mechanism for the formation of porous spheres is shown in Fig. 7. BA forms an aqueous microemulsion, which is substantiated by an observed laser Tyndall Effect. BuOH is miscible with both BA and water, but more favorably partitions into BA. The redox reaction between BuOH and $KMnO_4$ thus occurs inside the BA microemulsion, which serves as a receptacle and template for the manganese oxide nanoparticles. BA also plays the role of capping ligand for the nanopalatelets, limiting their growth. The observed dependence of sphere diameter on $KMnO_4$ concentration (Fig. 5) is a consequence of more nanoplatelets being formed within the microemulsion.

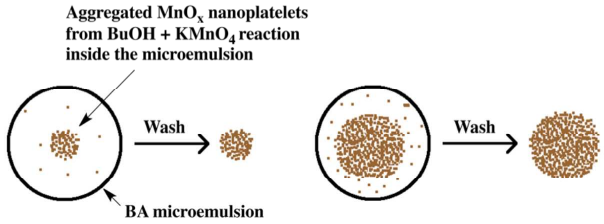

Fig. 7. Proposed mechanism for porous manganese oxide spheres. BuOH partitions into the BA microemulsion, where it undergoes reaction with $KMnO_4$. The resulting manganese oxide nanoparticles aggregate within the microemulsion to form a porous sphere. Higher $KMnO_4$ concentration yields more MnO_x nanoparticles and larger spheres.

This proposed mechanism is further supported by reactions carried out at higher and lower temperatures. SEM images of porous manganese oxide spheres prepared at 60 °C and 5 °C are shown in Fig. 8. Reactions at 60 °C yield highly monodiperse spheres, similar to observation at room temperature, but with much smaller diameters. Conversely, reactions at 5 °C produce spheres with much larger diameters, and there is noticable loss of monodispersity. The increase in sphere size with decreasing

reaction temperature is consistent with the trend in carboxylic acid miscibility with water. Lower temperature results in lower BA miscibility, resulting in larger-sized emulsion particles and ultimately larger manganese oxide spheres.

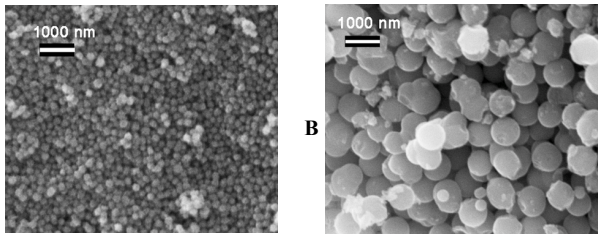

Fig. 8. SEM images of spheres (S1 procedure) at (A) 60 °C and (B) 5 °C. Spheres from the room temperature reaction are shown in Fig. 1A.

Reaction dwell times were also investigated. Filtration was used to abort reactions, while manganese oxide structures were still forming. SEM images of manganese oxide obtained after 4 and 8 minutes show the spherical morphology emerging even at the initial stages of reaction, S7. At 4 minutes, the spheres have smaller size compared to those from the completed reaction. At 8 minutes, the spheres are larger and the size goes unchanged at longer reaction times. In both cases, spheres are less well formed and less monodisperse relative to the normally obtained spheres. The decrease in uniformity is attributed to disruption of stirring and slow filtration in the aborted reactions.

The mechanism shown in Fig. 7 for manganese oxide *porous* spheres is consistent with what we proposed in a previously published communication on the synthesis of manganese oxide *hollow* spheres.[4] The latter were obtained by reacting MnO_4^- and Mn^{2+} in aqueous BA. The key difference in the reaction leading to hollow structures is that Mn^{2+} serves as the reducing agent, rather than BuOH, as reported here. Thus, both MnO_4^- and Mn^{2+} reside in the aqueous phase, and the resulting nanoplatelets form outside the BA microemulsion, aggregating on the surface to form a shell. This BA template is easily removed from the porous shell by washing, leaving behind the hollow sphere. By contrast, in the BA/BuOH system reported here, BuOH partitions into the BA microemulsion and reacts with $KMnO_4$ on the inside to form porous spheres comprised of aggregated nanoparticles, Fig. 7.

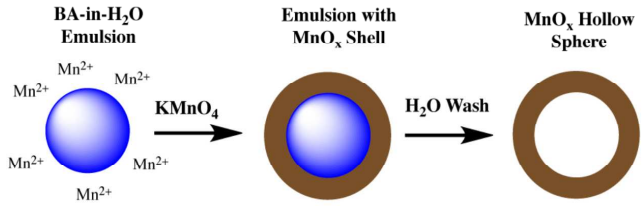

Fig. 9. Proposed mechanism for hollow manganese oxide spheres.[4] In this reaction, the reducing agent is Mn^{2+} instead of BuOH. Since both Mn^{2+} and MnO_4^- favor the aqueous phase. The reaction occurs outside the BA microemulsion and the resulting nanoparticles aggregate on the surface to form a shell. Washing removes the BA template.

Oleic acid has previously been reported to react with $KMnO_4$ in an oil-and-water emulsion that generates layered manganese oxide, which in turn aggregates into honeycomb or hollow sphere hierarchical morphologies, depending on $KMnO_4$ concentration.[16] This is a very slow reaction that involves oxidizing the C=C double bond of the water-insoluble oleic acid. There is no evidence of carboxylic acid coordination or other influences on particle size. Reactions between Mn^{2+} with $HMnO_4$ have also been shown to control the formation of γ-MnO_2 as hollow or solid spheres.[17] The type of hierarchical structure is determined by the rate of permanganic acid addition. Small particle size is reported, as well as the highest surface area for γ-MnO_2.

Reactions between $KMnO_4$ and smaller alcohols (MeOH, EtOH, PrOH) in aqueous BA generate materials that have morphologies resembling that of the control reaction between $KMnO_4$ and BuOH in the absence of BA, Fig. 4. This can be attributed to the greater miscibilty of smaller alcohols with water, favoring a reaction in the aqueous phase rather than in the BA microemulsion. However, hollow spheres are not observed either, indicating that nanoparticle aggregation occurs differently from the MnO_4^-/Mn^{2+} system, despite both reactions occuring in the aqueous phase. Longer chain alcohols such as various isomers of pentanol and hexanol are poorly soluble in water, but in small amounts they are viable reducing agents in preparing manganese oxide porous spheres. Work in this area is ongoing.

Isobutyric acid also forms aqueous microemulsions and can be utilized to prepare porous manganese oxide spheres, similar to BA. However, other carboxylic acids do not serve as good templates. Acetic acid and propionic acid do not form microemulsions, based on the lack of an observed Tyndall Effect. Their presence in the $KMnO_4$/BuOH reaction gives product similar to the control reaction without carboxylic acid. Longer chain carboxylic acids are poorly soluble in water and have not been successful in preparing monodisperse spheres.

Porous manganese oxide spheres are active catalysts for the oxidation of i-PrOH to acetone. Catalysis is carried out in the gas phase by bubbling a stream of He carrier gas with 1% O_2 through liquid i-PrOH. Conversion percentages range from 67% to 84% at 200 °C for different diameter spheres, Fig. 10. By comparison, manganese oxide prepared in a control reaction without BA converted only 40%. The enhanced activity may arise from the smaller particle size and higher surface area, which could translate into more active sites. This is particularly important if the sites are edges on the amorphous nanoplatelets, since these sites would increase considerably as platelet size decreases. The enhancement of oxidation catalysis aligns with results reported earlier for hollow spheres from our $KMnO_4/MnSO_4$/BA system and its ability to promote conversion of CO to CO_2.[4] Decreases in particle size and increases in surface area have been attributed to greater catalytic activity in the γ-MnO_2 system cited above,[17] which is also synthesized with both solid and hollow sphere morphologies. Additional catalytic studies are ongoing and beyond the scope of this communication.

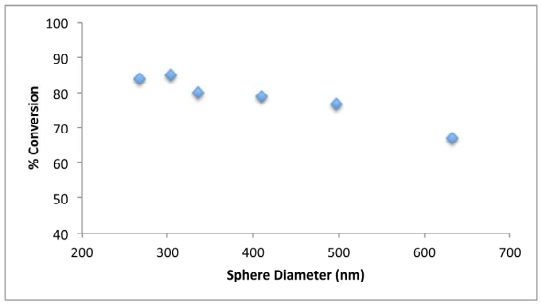

Fig. 10. Percent catalytic conversion of i-PrOH to acetone for porous manganese oxide spheres of varying diameters.

Conclusions

The reaction between $KMnO_4$ and BuOH in aqueous butyric acid provides a facile route to monodisperse manganese oxide porous spheres with tuneable diameters and high surface areas. The proposed mechanism has butyric acid serving both as a ligand that promotes nanoplatelet formation and a microemulsion that serves as a soft template for nanoparticle aggregation and sphere growth. Initial studies indicate that this is a promising material for oxidation catalysis.

Acknowledgments

We wish to acknowledge Jeff Carmichael, Nathan Giaccone, and Chrismary De La Cruz for technical assistance.

Notes and references

[a] *Department of Chemistry, Connecticut College, New London, CT 06320 USA. Fax: 860 439 2477; Tel: 860 439 2753; E-mail:sschi@conncoll.edu*
[b] *Current address: Department of Chemistry, University of Connecticut, Storrs, CT 06269 USA*

† Electronic Supplementary Information (ESI) available: Synthetic procedure for porous manganese oxide spheres, surface areas for different size spheres, SEM images of different size spheres.
See DOI: 10.1039/b000000x/

1 S. L. Suib, *J. Mater. Chem.*, 2008, **18**, 1623.
2 W. Wei, X. Cui, W. Chen and D. G. Ivey, *Chem. Soc. Rev*. **2011**, 40, 1697.
3 Y. Guo, H. Guo, Y. Wang, L. Liu and W. Chen, *RSC Adv.,* 2014, **4**, 14048.
4 S. Ching, D. A. Kriz, K. M. Luthy, E. C. Njagi and S. L. Suib, *Chem. Commun.*, 2011, **47**, 8286.
5 M. Toupin, T. Brousse and D. Belanger *Chem. Mater.*, 2004, **16**, 3184.
6 L. L. Yu, J. J. Zhu and J. T. Zhao, J. Mater. Chem. A, 2014, 2, 9353. (SA; porous)
7 Z. Li, Y. Ding, Y. Xiong, Q. Yang and Y. Xie, Chem. Comm., 2005, 918.
8 D. Portehault, S. Cassaignon, N. Nassif, E. Baudrin and J. P. Jolivet, *Angew. Chem. Int. Ed.*, 2008, **47**, 6441.
9 B. Li, G. Rong, Y. Xie, L. Huang and C. Feng, *Inorg. Chem.*, 2006, **45**, 6404.
10 X. He, M. Yang, P. Ni, Y. Li and Z.-H. Liu, Colloids Surf., A, 2010, 363, 64.
11 J. Wang, J. Liu, Y. Zhou, P. Hodgson and Y. Li, RSC Adv., 2013, 3, 25937.
12 X. Tang, Z. Liu, C. Zhang, Z. Yang and Z. Wang, *J. Power Sources*, 2009, **193**, 939.
13 N. Wang, Y. Gao, J. Gong, X. Ma, X. Zhang, Y. Guo and L. Qu, *Eur. J. Inorg. Chem*., 2008, 3827.
14 W. Zhang and Z. Zhang, *Chin. J. Chem. Phys*., 2009, **22**, 327.
15 P. Yu, X. Zhang, Y. Chen and Y. Ma, *Mater. Lett*., 2010, **64**, 1480.
16 H. Chen, J. He, C. Zhang and H. He, *J. Phys. Chem*. C, 2007, **111**, 18033.
17 J. Yuan, K. Laubernds, Q. Zhang and S. L. Suib, *J. Am. Chem. Soc.*, 2003, **125**, 4966.
18 G. Qiu, H. Huang, S. Dharmarathna, E. Benbow, L. Safford and S. L. Suib, *Chem. Mater.*, 2011, **23**, 3892.
19 R. Bagai and G. Christiou, *Chem. Soc. Rev.*, 2009, **38**, 1011.
20 R. Song, S. Feng, H. Wang and C. Hou, *J. Solid State Chem.*, 2013, **202**, 57.